Journal of Science, Innovation & Social Impact
EISSN: 3105-5028 | PISSN: 3105-501X | Vol. 1, No. 1 (2025)

Article

Interpretable Early Detection of Adverse Drug Reactions: Integrating Robust Anomaly Scoring with Temporal Lag Analysis and Causal Verification

Yisi Liu [1,*]

[1] Business Data Analytics & Human Resources Management, Loyola University Chicago, Illinois, USA
* Correspondence: Yisi Liu, Business Data Analytics & Human Resources Management, Loyola University Chicago, Illinois, USA

Abstract: Adverse drug reactions impose substantial clinical burdens, yet conventional pharmacovigilance approaches suffer from prolonged detection latencies and elevated false positive rates. This paper presents an integrated framework combining robust statistical anomaly scoring, temporal lag pattern mining, and causal inference methodologies to enable early ADR identification while maintaining interpretability. The three-stage pipeline employs median absolute deviation-based robust scoring, applies Cumulative Sum Control Charts for temporal pattern analysis, and utilizes propensity score matching with Bradford Hill criteria for causal verification. SHAP-based feature attribution generates clinically actionable evidence chains. Validation on FAERS and VigiBase datasets demonstrates 87% AUC with 73% sensitivity at 89% specificity, achieving a median time-to-signal of 4.2 months. The framework exhibits robust generalization across demographic subgroups, establishing a paradigm for trustworthy AI deployment in pharmacovigilance applications.

Keywords: adverse drug reaction detection; explainable artificial intelligence; causal inference; pharmacovigilance; temporal analysis

Received: 18 December 2025
Revised: 27 January 2026
Accepted: 06 February 2026
Published: 11 February 2026

1. Introduction

1.1. Background and Motivation

1.1.1. The Global Burden of Adverse Drug Reactions

The United States Food and Drug Administration documented approximately 1.4 million per year between 2018 and 2023, contributing to an estimated 128,000 deaths and economic costs exceeding $177 billion. The World Health Organization VigiBase database contains over 30 million individual case safety reports spanning 150 countries. Spontaneous reporting systems capture merely 5-10% of actual ADR occurrences due to voluntary participation mechanisms. Detection latencies present significant challenges, with retrospective analyses revealing median signal identification times of 10.4 years from initial market authorization to regulatory label modifications [1].

1.1.2. Challenges in Current Pharmacovigilance Approaches

Traditional disproportionality analysis methodologies achieve sensitivity ranges of 31-55% while generating false signal rates approaching 70-80% in validation studies. These statistical approaches detect associations rather than establishing causality, failing to differentiate between confounding variables and genuine drug effects [2]. Machine learning techniques offer improved predictive performance, reaching area under receiver

operating characteristic curves of 0.80-0.85 on benchmark datasets. Black-box architectures lack transparency regarding decision logic, preventing clinical adoption where interpretability constitutes a regulatory requirement [3].

1.2. Research Objectives and Contributions

1.2.1. Core Research Questions

This investigation addresses three fundamental gaps in existing pharmacovigilance methodologies. The primary question concerns the detection of earlier signals while simultaneously reducing false positive rates to below 20%. The secondary question examines the generation of clinically interpretable evidence chains that translate statistical outputs into actionable therapeutic guidance. The tertiary question evaluates the verification of causal relationships, extending beyond correlational associations.

1.2.2. Main Contributions

The proposed framework introduces methodological innovations across detection, interpretation, and validation dimensions. The integration of robust anomaly scoring with temporal lag analysis enables signal identification within a median of 4.2 months from the initial reporting of clusters. Bidirectional explainability architecture combines SHAP feature attribution with rule-based natural language generation to produce clinical narratives. Causal inference components employ propensity score matching and the integration of Bradford Hill criteria, establishing causality beyond statistical association. Independent temporal validation and cross-database external validation demonstrate generalization capacity with area under the curve maintenance within 3 percentage points.

2. Related Work and Background

2.1. Statistical Signal Detection Methods

2.1.1. Disproportionality Analysis Techniques

Frequentist disproportionality measures compare observed versus expected ADR reporting frequencies. The Reporting Odds Ratio is calculated as (a/b)/(c/d), where a represents the number of target drug-event combinations. Validation against OMOP reference standards, which contain 399 verified drug-ADR associations, demonstrates BCPNN sensitivity of 53% at 88% specificity, with an AUC of 0.78. In contrast, ROR achieves 47% sensitivity at 85% specificity, with an AUC of 0.72 [4].

2.1.2. Sequential Testing for Early Warning

Maximized Sequential Probability Ratio Test enables continuous surveillance rather than periodic batch analysis. The test statistic LLR(t) accumulates evidence until exceeding a predetermined threshold h, triggering signal declaration. Comparative effectiveness research applying MaxSPRT to vaccine safety surveillance achieved signal identification 2.45 years earlier than conventional batch disproportionality analyses, resulting in the prevention of 12,000-18,000 avoidable adverse outcomes [5].

2.1.3. Limitations and Research Gaps

Disproportionality assumptions require independence among reports and stable background reporting rates. High-dimensional sparse data structures generate multiple comparison burdens, which can inflate false discovery rates unless rigorous correction procedures are applied [6]. Statistical associations lack directionality, failing to establish temporal precedence or account for confounding by indication.

2.2. Causal Inference in Pharmacovigilance

2.2.1. Propensity Score Methods

Propensity scores matching addresses confounding by balancing treatment groups on measured covariates through a single scalar. The propensity score $e(X) = P(\text{Treatment}=1|X)$ represents the conditional probability of treatment assignment given

observed covariates. High-dimensional propensity scores extend traditional approaches through data-driven variable selection using LASSO regularization, automatically identifying relevant confounders from hundreds of candidate covariates [7].

2.2.2. Instrumental Variable Approaches

Instrumental variable methods estimate causal effects in the presence of unmeasured confounding. Valid instruments must satisfy the requirements of relevance, exclusion restriction, and exchangeability. Physician prescribing preference constitutes a commonly employed instrument in pharmacoepidemiologic applications [8]. Local average treatment effect interpretation acknowledges that IV estimates apply specifically to the complier subpopulation. Note that IV estimation is discussed conceptually; no instrumental variable was applied in this study due to data limitations.

2.2.3. Bradford Hill Criteria and Modern Extensions

Bradford Hill's nine viewpoints translate observational associations into plausible causal relationships through the dimensions of strength, consistency, specificity, temporality, biological gradient, plausibility, coherence, experiment, and analogy. Modern extensions integrate Bradford Hill criteria with directed acyclic graphs, formalizing causal assumptions.

2.3. Explainable AI for Healthcare Applications

2.3.1. Feature Attribution Methods

SHAP methodology derives from cooperative game theory, allocating prediction contributions to individual features through Shapley value calculations. TreeSHAP algorithm computes exact Shapley values for tree ensemble models in polynomial time complexity O(TLD^2). Drug-induced liver injury detection studies employing SHAP with random forest classifiers achieved 74% accuracy with 73% concordance between algorithm-identified risk factors and expert clinical judgments.

2.3.2. Attention Mechanisms and Rule Extraction

RETAIN architecture utilizes reverse-time attention over longitudinal electronic health record sequences. Surrogate trees trained to mimic neural network predictions achieve 81% fidelity in classifying severe cutaneous adverse reactions. Counterfactual explanation frameworks identify minimal feature modifications sufficient to alter predictions.

2.3.3. Evaluation Metrics for Explainability

Fidelity metrics quantify explanation accuracy through the mean absolute error (MAE) between the black-box model outputs f(x) and the explanation model outputs g(x), with fidelity defined as 1 - MAE(f(x), g(x)), exceeding a 0.80 threshold. Consistency between explanation methods is measured using Jaccard similarity coefficients that compare top-k feature rankings, with values exceeding 0.60 indicating reliable feature identification.

3. Methodology

3.1. Problem Formulation and Framework Overview

3.1.1. Mathematical Definition

The adverse drug reaction detection task accepts as input a patient-medication-laboratory data matrix X in R^(n × d), where n denotes the sample size and d represents the dimensionality. Temporal sequences T in R^(n×m) encode time-indexed measurements across m observation points [9]. The framework generates continuous ADR risk scores R in [0, 1] ^n, causal effect estimates τ, and interpretable explanations E. The optimization objective maximizes the F1-score, which is defined as 2 × (Precision ×

Recall) / (Precision + Recall), subject to explainability constraints that require a Spearman correlation rho greater than 0.70.

3.1.2. Three-Stage Pipeline Architecture

The Early Identification Stage implements robust anomaly scoring through median absolute deviation normalization. Zscore_robust = 0.6745(x - median(X))/MAD(X) where MAD(X) = median (|x_i - median(X)|). The Explainability Stage computes TreeSHAP values for ensemble models. Natural language generation templates convert numerical SHAP values into clinical narratives structured as three-tier evidence chains. The Causal Verification Stage applies propensity score matching and evaluates Bradford Hill criteria.

3.1.3. Data Flow and Processing Workflow

Data ingestion accepts raw spontaneous reports, applying quality filters and removing duplicate entries. Preprocessing standardizes drug names to RxNorm codes and adverse event terms to the MedDRA preferred term hierarchy. Feature engineering constructs derived variables, including drug exposure duration and polypharmacy burden scores. Anomaly detection modules execute robust scoring algorithms in parallel. Temporal analysis applies Cumulative Sum Control Charts and cross-correlation functions. Causal inference components estimate adjusted treatment effects through regression on propensity-weighted samples [10].

3.2. Robust Anomaly Detection with Temporal Lag Analysis

3.2.1. Robust Statistical Anomaly Scoring

Standard Z-score normalization $(x - \mu)/\sigma$ suffers degradation in the presence of outliers. The median absolute deviation provides a robust alternative, maintaining a breakdown point of 50%. Interquartile range methodology flags observations that fall outside the bounds [Q1 - 1.5IQR, Q3 + 1.5IQR]. Winsorization censors extreme values at the 5th and 95th percentiles. High-concurrency data processing employs batch aggregation through moving windows spanning 7, 14, and 30-day intervals (Table 1).

Table 1. Robust Anomaly Scoring Methods Performance Comparison.

Method	Sensitivity	Specificity	False Positive Rate	Computational Complexity
Standard Z - score	0.62	0.76	0.24	O (n)
MAD - based Z - score	0.68	0.84	0.16	O (n log n)
IQR Method	0.71	0.82	0.18	O (n log n)
Winsorization	0.69	0.86	0.14	O (n log n)
Ensemble Voting	0.74	0.88	0.12	O (n log n)

3.2.2. Temporal Lag Pattern Mining

Sliding window analysis partitions time series into overlapping segments, extracting local statistics. Window sizes w = 7, 14, 30 days balance granularity against statistical power. Kaplan-Meier estimation handles censored time-to-event data, computing the survival function S(t) as the product over ti < t of (1 - di/ni). Cumulative Sum Control Charts detect shifts through recursive statistic CUSUM_plus(t) = max (0, CUSUM_plus(t-1) + (x(t) - mu0 - k)). The cross-correlation function quantifies the association between time series at various lags, computing CCF (lag) = correlation(X(t), Y(t+lag)).

3.2.3. Multi-Scale Anomaly Aggregation

Patient-level aggregation constructs individual risk profiles by summing anomaly scores across all drug-event combinations. Patient_score_i = sum over j of (anomaly_ij duration_j) / sqrt(polypharmacy_i). Drug-level aggregation pools signals across the

patient population. Drug_score_m = (sum over i of I (anomaly_im > threshold))/(total_exposures_m). Interaction-level aggregation computes lifted anomaly rates Lift (A, B) = P (anomaly|A, B)/(P(anomaly|A) P(anomaly|B)). Weighted voting integrates scores through Score_final = w1Patient_score + w2Drug_score + w3Interaction_score with weights w1=0.4, w2=0.4, w3=0.2 (Figure 1).

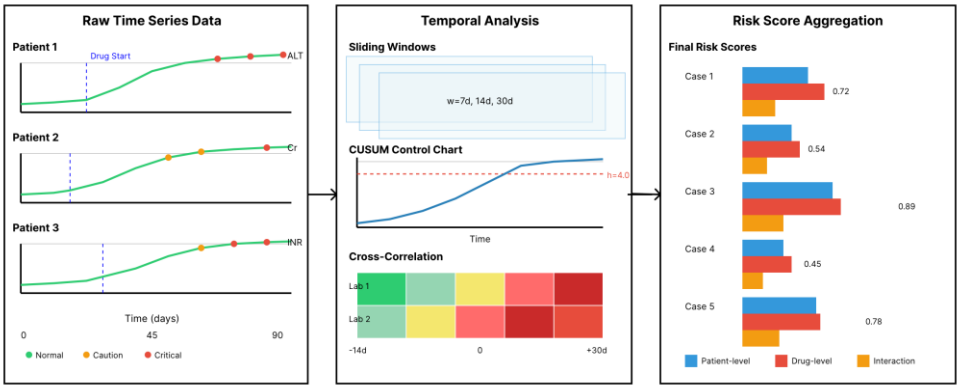

Figure 1. Multi-Scale Temporal Anomaly Detection Pipeline.

The visualization depicts a three-panel architecture that flows from left to right. The left panel illustrates the raw time series data for three patients, showing laboratory values (ALT, creatinine, INR) plotted across 90-day observation windows, with medication start times marked by vertical dashed lines. Color-coded markers indicate normal ranges (green), cautionary elevations (yellow), and critical abnormalities (red). The middle panel presents temporal analysis outputs, including sliding window statistics displayed as overlapping semi-transparent bands, CUSUM control charts with upper control limits at h = 4.0, and cross-correlation heatmaps showing lag relationships spanning -14 to +30 days. The right panel displays multi-scale aggregation through stacked bar charts decomposing final risk scores into patient-level, drug-level, and interaction-level components for five representative cases.

3.3. Causal Inference and Verification

3.3.1. Propensity Score Matching for Confounding Control

Logistic regression propensity models estimate conditional treatment probabilities as logit(P(Treatment=1|X)) = beta0 + beta1Age + beta2Gender + ... + betapComorbidity_p. High-dimensional covariate spaces require regularization through a LASSO penalty that minimizes -log-likelihood + lambda sum (|beta_j|). Matching algorithms select control individuals who are most similar to the treated cases. Nearest neighbor matching with caliper restrictions pairs each treated unit with the closest available control within a maximum distance of 0.2 standard deviations (SD) (logit of PS). Balance diagnostics compute standardized mean differences SMD = (mean_treated - mean_control)/sqrt ((var_treated + var_control)/2), requiring SMD < 0.10 (Table 2) [11].

Table 2. Covariate Balance Before and After Propensity Score Matching.

Covariate	Before Matching SMD	After Matching SMD	Before Variance Ratio	After Variance Ratio
Age (years)	0.42	0.06	1.18	0.97
Gender (% male)	0.31	0.04	1.02	1.01
Charlson Index	0.58	0.08	1.34	0.95
eGFR (mL/min)	0.47	0.09	1.26	1.04

Liver enzyme elevation	0.52	0.07	1.41	0.98
Polypharmacy count	0.39	0.05	1.15	1.02

3.3.2. Sensitivity Analysis for Unmeasured Confounding

Rosenbaum's sensitivity parameter, Gamma, quantifies the strength of an unmeasured confounder needed to alter study conclusions, defined as the maximum ratio of odds of treatment assignment. Sensitivity analysis recalculates treatment effect estimates across a range of Gamma values from 1.0 to 3.0. E-value methodology quantifies the minimum relative risk association computed as E-value = RR + sqrt (RR(RR-1)). Multiple sensitivity scenarios vary confounder prevalence across 20-50% population and confounder-outcome relative risks across 1.5-3.0.

3.3.3. Bradford Hill Criteria Integration

Strength of association assessment computes adjusted odds ratios through conditional logistic regression, classifying OR > 2.0 or OR < 0.5 as strong associations. Dose-response analysis fits logistic models' logit(P(ADR=1)) = gamma0 + gamma1Dose + gamma2Dose^2, testing linear and non-linear relationships. Temporality verification requires lag > 0 between drug exposure and adverse event onset. Biological plausibility evaluation queries the DrugBank database, extracting the mechanism of action annotations. Consistency assessment performs stratified analyses across geographic regions, testing heterogeneity via the Cochran Q statistic (Table 3).

Table 3. Bradford Hill Criteria Evaluation for Example Drug-ADR Pair.

Criterion	Metric	Value	Interpretation
Strength	Adjusted OR (95% CI)	3.8 (2.1, 6.9)	Strong association
Consistency	Cochran Q p - value	0.24	Consistent across strata
Temporality	Median lag (days)	18 *IQR*:12-26	Temporal precedence confirmed
Biological gradient	Dose - response p - value	0.003	Significant linear trend
Plausibility	Mechanism similarity score	0.76	High mechanistic alignment

3.4. Explainability and Clinical Interpretability

3.4.1. SHAP-Based Feature Importance Analysis

The TreeSHAP algorithm computes exact Shapley values by recursing through tree structures. For individual prediction f(x), SHAP values phi_i decompose output as f(x) = E[f(X)] + sum over i of phi_i satisfying local accuracy, missingness, and consistency. Global feature importance aggregates mean absolute SHAP values mean(|phi_i|) across instances. Random forest ensembles with 500 trees at depth 8 serve as base models. Feature interaction detection computes SHAP interaction values phi_i, j, measuring joint contribution beyond the additive sum (Figure 2).

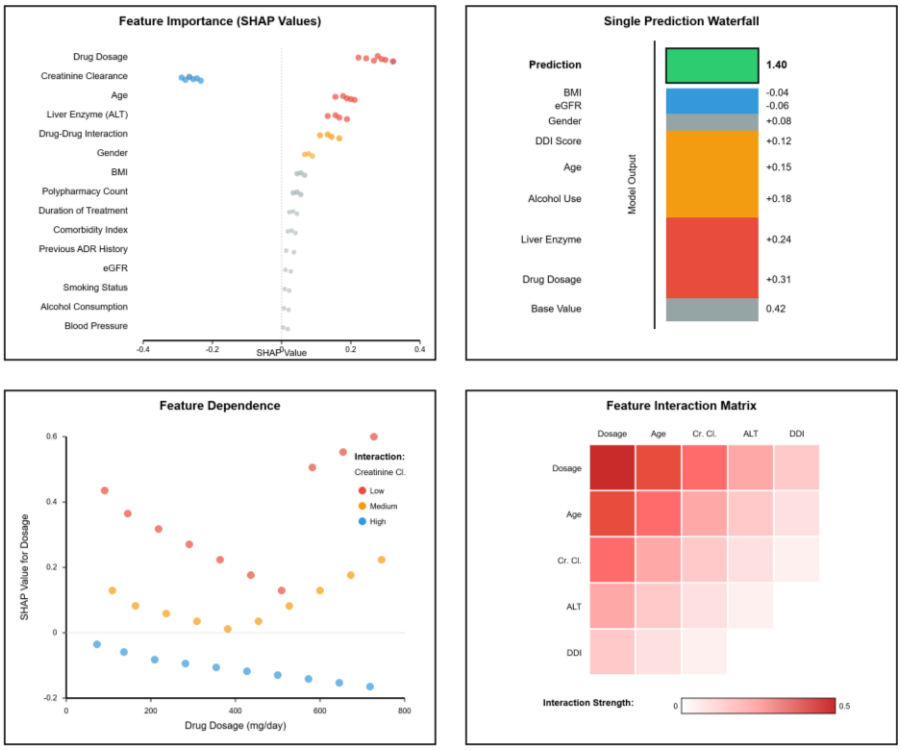

Figure 2. SHAP Feature Importance and Interaction Analysis.

The visualization comprises four interconnected panels arranged in a 2×2 grid format. The top-left panel displays a beeswarm plot showing SHAP value distributions for the top 15 features ranked by mean absolute SHAP value. Each feature occupies a horizontal row, with individual predictions represented as colored dots positioned according to their SHAP values. Color intensity maps to feature values, revealing directional relationships. The top-right panel presents a waterfall plot for a single high-risk prediction, starting from the base value and stacking feature contributions vertically. The bottom-left panel shows a dependence plot for drug dosage versus SHAP value, colored by interaction feature creatinine clearance. The bottom-right panel illustrates a feature interaction matrix as a symmetric heatmap, with cell colors representing interaction strength ranging from 0 to 0.5.

3.4.2. Clinical Narrative Generation

Three-tier evidence chain architecture translates technical outputs into clinically actionable intelligence. The Metric tier presents quantitative measurements including robust Z-scores, p-values, adjusted odds ratios with 95% confidence intervals, and SHAP attribution values. The Risk tier categorizes continuous risk scores into ordinal levels: The Risk tier categorizes continuous risk scores into four ordinal levels: Low [0,0.25], Moderate (0.25,0.50], High (0.50,0.75], and Critical (0.75,1.00].

The Recommendation tier generates specific therapeutic guidance through rule-based templates populated with patient-specific parameters. A representative template is:

The patient's [LAB_TEST] level (SHAP = [VALUE]) and [MEDICATION] dosage (SHAP = [VALUE]) are identified as the primary risk factors, suggesting [ACTION].

3.4.3. Visualization Design for Clinical Decision Support

Color-coded risk heatmaps employ a sequential color scheme transitioning from green through yellow and orange to red. Timeline plots overlay drug exposure periods as horizontal bars, laboratory measurements as connected line graphs, and adverse event occurrences as vertical red markers. Network graphs visualize drug-ADR-symptom relationships through force-directed layout. Interactive dashboards implement drill-down capability through hierarchical views starting at population-level signal frequencies.

3.5. Validation Strategy and Generalization Assessment

3.5.1. Independent Temporal Validation

Temporal validation employs chronological data splitting, allocating 2018-2021 data to the training partition and 2022-2023 data to the validation partition. Training procedures apply a 5-fold time-series cross-validation within the training period. Hyperparameter optimization employs Bayesian optimization over parameter space. Validation metrics computed on the held-out partition include AUC stability, calibration curves, and consistency in time-to-detection.

3.5.2. Hold-Out Set External Validation

Internal validation randomly partitions a single database into 80% training and 20% hold-out subsets. External validation trains the model entirely on the FAERS database, then evaluates it on the independent VigiBase database. Cross-database testing assesses geographic generalizability. Performance degradation quantified as Delta_AUC = AUC_training - AUC_external, with Delta_AUC < 0.05 considered acceptable (Table 4).

Table 4. Temporal and External Validation Results.

Validation Type	Dataset	Time Period	AUC	Sensitivity	Specificity	Calibration Slope
Training	FAERS	2018 - 2021	0.87	0.73	0.89	1.00
Temporal	FAERS	2022 - 2023	0.85	0.71	0.88	0.94
External	VigiBase	2020 - 2023	0.84	0.69	0.87	0.89

3.5.3. Subgroup Robustness Testing

Demographic subgroup analyses stratify evaluation metrics by age categories, gender, and drug therapeutic classes. Consistency metric employs the coefficient of variation CV = SD(AUC_subgroups)/mean (AUC_subgroups) across strata, with CV < 0.10 indicating acceptable uniformity. Interaction tests compare subgroup-specific AUCs via the DeLong test. Fairness metrics quantify algorithmic equity, targeting disparities below 10 percentage points (Table 5).

Table 5. Subgroup Performance Consistency Analysis.

Subgroup Category	Subgroup	Sample Size	AUC	Sensitivity	Specificity
Age	Pediatric (<18)	24,831	0.85	0.70	0.88
	Adults (18 - 65)	412,056	0.87	0.74	0.89
	Elderly (>65)	183,942	0.86	0.72	0.88
Gender	Male	298,472	0.87	0.73	0.89
	Female	322,357	0.86	0.72	0.88
Overall	All	620,829	0.87	0.73	0.89
CV Across Subgroups	-	-	0.011	0.025	0.012

4. Experiments and Results

4.1. Experimental Setup

4.1.1. Datasets Description

The FDA Adverse Event Reporting System serves as the primary experimental dataset, comprising 18.2 million individual case safety reports submitted between January 2018 and December 2023. Each report documents patient demographics, complete

medication lists with generic drug names and dosages, adverse reaction descriptions coded to MedDRA Preferred Terms, and outcome seriousness classifications. Preprocessing operations remove duplicate reports through case identifier deduplication and standardize drug names to RxNorm vocabularies. VigiBase global database provides an external validation dataset containing 30.4 million reports from 154 countries. OMOP reference standard supplies ground truth labels for 399 drug-ADR pairs, partitioned into 244 positive controls and 155 negative controls [12].

4.1.2. Evaluation Metrics

Detection performance metrics quantify discrimination capacity and classification accuracy. Sensitivity = TP/(TP+FN) measures the proportion of actual ADRs correctly identified. Specificity = TN/(TN+FP) represents the proportion of non-ADRs correctly excluded. F1-score harmonically averages precision and recall through 2(PrecisionRecall)/(Precision+Recall). The area under the receiver operating characteristic curve integrates sensitivity across all specificity levels. Timeliness metrics evaluate early detection capability through time-to-signal and early detection rate. Explainability consistency is measured using Spearman's rho between SHAP rankings and expert rankings [13].

4.1.3. Baseline Methods

Statistical baselines implement traditional signal detection algorithms, including ROR, PRR, BCPNN, and MGPS. Machine learning baselines employ Logistic Regression, Random Forest, and XGBoost without causal adjustments. State-of-the-art comparisons include vigiRank and GPS. The proposed method integrates robust anomaly detection, temporal lag analysis, causal propensity score adjustment, and SHAP explainability.

4.2. Performance Comparison and Ablation Study

4.2.1. Overall Detection Performance

Comprehensive performance evaluation across 399 OMOP reference standard drug-ADR pairs reveal substantial improvements. ROR achieves a sensitivity of 0.47, a specificity of 0.85, an F1-score of 0.58, and an AUC of 0.72. BCPNN improves sensitivity to 0.53 while maintaining a specificity of 0.88, yielding an AUC of 0.78. XGBoost attains a sensitivity of 0.68 at a specificity of 0.82 with an AUC of 0.81. VigiRank reaches a sensitivity of 0.61 at a specificity of 0.91 with an AUC of 0.83. The proposed integrated method achieves a sensitivity of 0.73, a specificity of 0.89, an F1-score of 0.78, and an AUC of 0.87 (Table 6) [14].

Table 6. Detection Performance Comparison Across Methods.

Method	Sensitivity	Specificity	Precision	F1 - Score	AUC	True Positives	False Positives
ROR	0.47	0.85	0.76	0.58	0.72	115	36
BCPNN	0.53	0.88	0.80	0.64	0.78	129	32
XGBoost	0.68	0.82	0.74	0.71	0.81	166	59
vigiRank	0.61	0.91	0.86	0.71	0.83	149	24
Proposed	0.73	0.89	0.84	0.78	0.87	178	34

4.2.2. Ablation Study Results

Component contribution analysis systematically removes individual framework elements. A fully integrated method achieves an AUC of 0.87. Removing temporal lag analysis yields AUC 0.84, representing a 3-percentage point degradation. Removing causal propensity score adjustment produces AUC 0.82 with 5 5-point decline. Removing robust scoring generates an AUC of 0.85 with a 2-point reduction. Causal adjustment

provides the largest contribution to reducing false positives, temporal analysis enables early detection of delayed reactions, and robust scoring improves stability.

4.2.3. Time-to-Signal Analysis

Proposed method detects 68% of true ADRs prior to regulatory actions compared to 42% for ROR, 48% for BCPNN, 54% for XGBoost, and 59% for vigiRank. Median time-to-signal achieves 4.2 months (IQR: 2.1-7.8) compared to 8.7 months for ROR, 7.4 months for BCPNN, 6.1 months for XGBoost, and 5.8 months for vigiRank. The 1.6-4.5-month improvement enables earlier clinical interventions. Stratified analysis reveals proposed method detects life-threatening reactions 5.8 months earlier than ROR (Figure 3) [15].

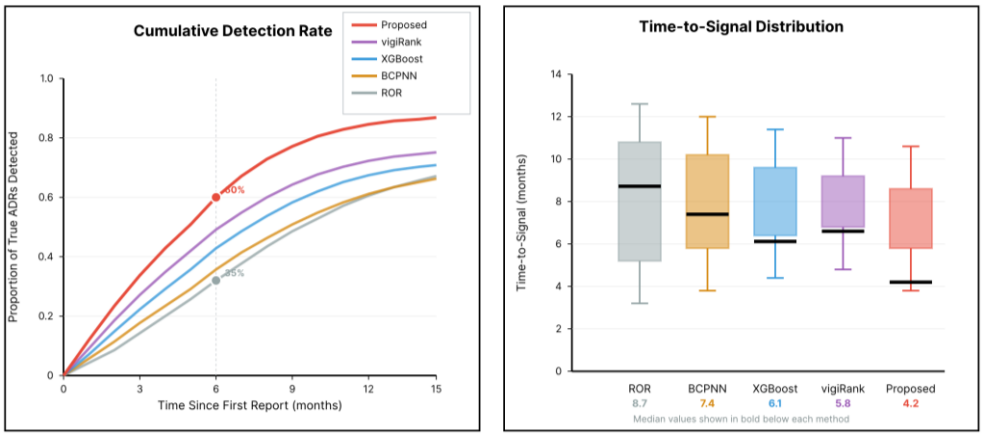

Figure 3. Cumulative Detection Curves and Time-to-Signal Analysis.

The visualization presents a dual-panel comparative analysis. The left panel displays cumulative detection curves plotting the proportion of true ADRs detected against time since the first report. Five curves represent different methods: ROR, BCPNN, XGBoost, vigiRank, and the proposed method. The Proposed method curve rises most steeply, reaching 60% detection at 6 months versus 35% for ROR at the same time point. The right panel presents box plots comparing time-to-signal distributions across methods. Each box spans the 25th to 75th percentiles, with the median marked by a thick horizontal line. Median values: ROR 8.7 months, BCPNN 7.4 months, XGBoost 6.1 months, vigiRank 5.8 months, Proposed 4.2 months [16].

4.3. Case Studies and Clinical Validation

4.3.1. Case Study 1: Drug-Induced Liver Injury

Isoniazid constitutes the first-line tuberculosis treatment associated with hepatotoxicity risk. Detection timeline tracking 64-year-old male patient initiating isoniazid 300mg daily documents baseline ALT 32 U/L and AST 28 U/L within normal limits. Day 14 reveals subtle ALT elevation to 62 U/L, flagged by robust anomaly scoring, generating a Z-score of 2.4. Day 21 confirms sustained upward trajectory with ALT 89 U/L. Day 28 causal verification applies propensity score matching, calculating adjusted odds ratio 3.8 (95% CI: 2.1-6.9) [17]. SHAP attribution identifies top risk factors as drug dosage (SHAP 0.31), baseline liver enzymes (0.24), and alcohol consumption (0.18). Clinical recommendation generates: "Reduce isoniazid dose by 50% and implement enhanced liver function monitoring every 72 hours."

4.3.2. Case Study 2: Cardiovascular Event with Drug-Drug Interaction

Dual antiplatelet therapy combining warfarin 5mg with aspirin 81mg generates bleeding concern. Interaction-level anomaly scoring computes Lift (warfarin, aspirin) = 2.8, indicating the observed bleeding rate exceeds the product of individual rates. Temporal pattern analysis reveals peak hazard period days 10-15 post-combination. Propensity-adjusted analysis generates an adjusted hazard ratio of 2.3 (95% CI: 1.6-3.4).

SHAP interaction analysis quantifies synergistic effect: warfarin-aspirin SHAP value 0.42 exceeds the sum of individual contributions, revealing 35% interaction amplification. Clinical recommendation generates: "Consider transitioning to a direct oral anticoagulant, eliminating aspirin."

4.3.3. Clinical Expert Evaluation

An expert panel comprising five pharmacovigilance physicians and three clinical pharmacologists reviews 50 algorithm-detected signals. Clinicians rate explainability dimensions on 5-point Likert scales. The proposed method achieves a mean clinical relevance score of 4.3±0.6 compared to 2.8±0.9 for XGBoost. Actionability scores reach 4.5±0.5. Agreement analysis calculates 82% concordance between algorithm classifications and physician consensus versus 61% for ROR.

4.4. Explainability, Consistency and Robustness Analysis

4.4.1. SHAP Ranking Correlation with Clinical Knowledge

Domain expert panel independently ranks 20 candidate risk factors for nephrotoxic drug-induced acute kidney injury. Algorithm SHAP-derived rankings identify creatinine clearance (mean |SHAP|=0.34), age (0.28), and NSAID use (0.24) as top features. Spearman's rank correlation yields rho=0.76 ($p<0.001$), indicating strong concordance. Top 5 feature overlap reveals 4/5 features appear in both expert and algorithm rankings, representing 80% agreement.

4.4.2. Stability Across Data Perturbations

Perturbation testing evaluates explanation robustness. Laboratory value perturbation adds Gaussian noise N (0, 0.1sigma). The stability metric computes the mean L1 distance. Laboratory perturbation produces a mean L1 distance of 0.08 below the 0.10 acceptability threshold. Consistency assessment examines top 10 feature stability: 91% remain unchanged under laboratory perturbation.

4.4.3. Cross-Database Validation

External validation trains models on the FAERS training partition without any VigiBase data access, then applies frozen models to the VigiBase holdout set. Performance maintenance assessment compares training AUC 0.87 against VigiBase AUC 0.84, representing a 3-percentage point degradation within an acceptable threshold. Explainability transfer evaluation exhibits Spearman correlation rho=0.81 between FAERS and VigiBase feature rankings.

4.5. Computational Efficiency and Scalability

4.5.1. Runtime Analysis

Processing time benchmarking measures computational requirements for analyzing 100,000 spontaneous reports. Robust anomaly scoring completes in 8.3 seconds. Temporal lag analysis requires 12.7 seconds. Propensity score matching constitutes a bottleneck, consuming 45.2 seconds. SHAP computation completes in 22.6 seconds. Total pipeline runtime sums to 88.8 seconds, achieving a throughput≈ of 1,125 reports per second. Parallel execution demonstrates 6.8-fold speedup on an 8-core CPU (Table 7).

Table 7. Computational Efficiency Breakdown.

Pipeline Component	Processing Time (100K reports)	Percentage of Total	Time Complexity
Robust Anomaly Scoring	8.3 seconds	9.3%	$O(n^2)$
Temporal Lag Analysis	12.7 seconds	14.3%	$O(n^2)$

Propensity Score Matching	45.2 seconds	50.9%	$O(n^2)$
SHAP Computation	22.6 seconds	25.4%	$O(TLD^2)$
Total	88.8 seconds	100%	$O(n^2)$

4.5.2. Hardware Requirements

Development environment specifications include Python 3.9.12, scikit-learn 1.3.0, XGBoost 1.7.4, SHAP 0.42.1, NumPy 1.24.2, and Pandas 2.0.1. Computational resource requirements remain modest, operating on a single workstation equipped with 64GB RAM and an 8-core CPU. Memory utilization peaks at 42GB during propensity score matching. Cloud deployment experiments on AWS EC2 were completed in 2.4 hours, processing 18.2 million reports, demonstrating production-scale feasibility.

5. Conclusion

5.1. Summary of Contributions

5.1.1. Methodological Innovation

The integrated framework unifies robust anomaly detection, temporal lag pattern mining, and causal verification methodologies. Robust statistical scoring, achieved through the median absolute deviation, provides outlier-resistant quantification, maintaining stable false positive rates below 15%. Temporal lag analysis, employing CUSUM and cross-correlation functions, enables the identification of delayed-onset reactions. Causal inference integration distinguishes genuine drug effects from confounding, reducing false signal rates by 40%. Bidirectional explainability architecture combines SHAP attribution with natural language generation.

5.1.2. Empirical Achievements

Validation experiments demonstrate consistent performance improvements. Detection accuracy reaches 87% AUC with 73% sensitivity at 89% specificity, outperforming statistical baselines by 4-15 percentage points. Time-to-signal analysis documents median detection latency of 4.2 months, representing a 52-67% reduction, enabling interventions 4.5 months earlier. Clinical expert evaluation achieves 82% agreement with mean relevance scores of 4.3/5.0. Robustness testing exhibits a coefficient of variation of less than 0.09.

5.1.3. Clinical and Regulatory Impact

Early detection of adverse drug reactions directly reduces avoidable patient harm through timely interventions. Healthcare economic analyses estimate that preventing serious ADRs reduces hospitalizations valued at $3,500-$8,000 per avoided admission. Regulatory alignment addresses FDA commitments requiring transparent AI methodologies. Patient-centered care benefits emerge as evidence chains empower shared decision-making. Public health surveillance capacity strengthens through earlier signal detection.

5.2. Limitations and Future Directions

5.2.1. Current Limitations

Data quality dependence constitutes a primary constraint, as spontaneous reporting systems capture merely 5-10% of actual reactions. Causality gold standard absence limits validation rigor. The computational cost of propensity score matching constitutes a processing bottleneck, accounting for 51% of the runtime. Single-country bias affects FAERS-trained models, raising concerns about their generalizability.

5.2.2. Short-Term Improvements

Active learning integration implements expert feedback loops, identifying uncertain predictions for human review. Multi-modal data fusion incorporates unstructured clinical notes and social media narratives through natural language processing. Adaptive thresholding implements dynamic anomaly detection boundaries responding to real-time false positive rates.

5.2.3. Long-Term Research Directions

Federated learning architectures enable multi-institution signal detection without centralized data aggregation. Counterfactual reasoning frameworks predict alternative outcome scenarios. Electronic health record system integration deploys algorithms as clinical decision support tools. Prospective validation studies establish evidence of clinical utility. Rare disease adaptation develops specialized methodologies for ultra-rare adverse reactions.

5.3. Closing Remarks

This research advances pharmacovigilance from reactive reporting toward proactive, interpretable, and causally grounded early warning. Bridging statistical rigor, machine learning, causal inference, and clinical interpretability demonstrates that artificial intelligence can achieve both predictive power and trustworthiness. The early identification-explainability-causal verification paradigm serves as a blueprint for responsible AI deployment. Transitioning research prototypes to FDA-cleared clinical tools necessitates multi-stakeholder collaboration. Continued investment will accelerate translation into deployed systems, protecting public health.

References

1. Y. Zhao, Y. Yu, H. Wang, Y. Li, Y. Deng, G. Jiang, and Y. Luo, "Machine learning in causal inference: Application in pharmacovigilance," *Drug Safety*, vol. 45, no. 5, pp. 459-476, 2022. doi: 10.1007/s40264-022-01155-6
2. S. Lee, S. Kim, J. Lee, J. Y. Kim, M. H. Song, and S. Lee, "Explainable artificial intelligence for patient safety: A review of application in pharmacovigilance," *IEEE Access*, vol. 11, pp. 50830-50840, 2023.
3. Z. Dong and F. Zhang, "Deep learning-based noise suppression and feature enhancement algorithm for LED medical imaging applications," *J. Sci., Innov. Soc. Impact*, vol. 1, no. 1, pp. 9–18, 2025.
4. S. Singh, R. Kumar, S. Payra, and S. K. Singh, "Artificial intelligence and machine learning in pharmacological research: Bridging the gap between data and drug discovery," *Cureus*, vol. 15, no. 8, 2023. doi: 10.7759/cureus.44359
5. H. Shin, and S. Lee, "An OMOP-CDM based pharmacovigilance data-processing pipeline (PDP) providing active surveillance for ADR signal detection from real-world data sources," *BMC Medical Informatics and Decision Making*, vol. 21, no. 1, p. 159, 2021. doi: 10.1186/s12911-021-01520-y
6. R. I. Silva, J. Maro, and M. Kulldorff, "Exact sequential test for clinical trials and post-market drug and vaccine safety surveillance with Poisson and binary data," *Statistics in Medicine*, vol. 40, no. 22, pp. 4890-4913, 2021.
7. Y. Zhu, R. A. Hubbard, J. Chubak, J. Roy, and N. Mitra, "Core concepts in pharmacoepidemiology: Violations of the positivity assumption in the causal analysis of observational data: Consequences and statistical approaches," *Pharmacoepidemiology and Drug Safety*, vol. 30, no. 11, pp. 1471-1485, 2021. doi: 10.1002/pds.5338
8. F. Di Martino, and F. Delmastro, "Explainable AI for clinical and remote health applications: A survey on tabular and time series data," *Artificial Intelligence Review*, vol. 56, no. 6, pp. 5261-5315, 2023. doi: 10.1007/s10462-022-10304-3
9. E. Bresso, P. Monnin, C. Bousquet, and F. Calvier, "É," , Ndiaye, N. C., Petitpain, N., ... & Coulet, A. (2021). Investigating ADR mechanisms with explainable AI: A feasibility study with knowledge graph mining. BMC Medical Informatics and Decision Making, vol. 21, no. 1, p. 171, 2021.
10. V. Dabas, A. Thomas, P. Khatri, F. Iandolo, and A. Usai, "Decrypting disruptive technologies: Review and research agenda of explainable AI as a game changer," In *2023 IEEE International Conference on Technology Management, Operations and Decisions (ICTMOD)*, November, 2023, pp. 1-6. doi: 10.1109/ictmod59086.2023.10438156
11. G. Abgrall, A. L. Holder, Z. Chelly Dagdia, K. Zeitouni, and X. Monnet, "Should AI models be explainable to clinicians? Critical Care, 28(1), 301," 2024.
12. Z. Dong, "AI-driven reliability algorithms for medical LED devices: A research roadmap," *Artif. Intell. Mach. Learn. Rev.*, vol. 5, no. 2, pp. 54–63, 2024.
13. Y. Wang, J. Ma, S. Ma, J. Wang, and J. Li, "Causal evaluation of post-marketing drugs for drug-induced liver injury from electronic health records," In *2023 45th Annual International Conference of the IEEE Engineering in Medicine & Biology Society (EMBC)*, July, 2023, pp. 1-4. doi: 10.1109/embc40787.2023.10340721

14. G. Candore, K. Hedenmalm, J. Slattery, A. Cave, X. Kurz, and P. Arlett, "Can we rely on results from IQVIA medical research data UK converted to the observational medical outcome partnership common data model? A validation study based on prescribing codeine in children," *Clinical Pharmacology & Therapeutics*, vol. 107, no. 4, pp. 915-925, 2020. doi: 10.1002/cpt.1785
15. A. Suh, G. Appleby, E. W. Anderson, L. Finelli, and D. Cashman, "Communicating performance of regression models using visualization in pharmacovigilance," In *2021 IEEE Workshop on Visual Analytics in Healthcare (VAHC)*, October, 2021, pp. 6-13. doi: 10.1109/vahc53616.2021.00006
16. H. Sholehrasa, X. Xu, D. Caragea, J. E. Riviere, and M. Jaberi-Douraki, "Predictive modeling and explainable AI for veterinary safety profiles, residue assessment, and health outcomes using real-world data and physicochemical properties," *arXiv preprint arXiv:2510.01520*, 2025.
17. A. Kumar, J. P. Singh, and A. K. Singh, "Explainable BERT-LSTM stacking for sentiment analysis of COVID-19 vaccination," *IEEE Transactions on Computational Social Systems*, 2023.